Pergamon   **PII: S0022-4073(98)00027-2**

COMBINED CONDUCTION AND RADIATION HEAT TRANSFER IN PLANE-PARALLEL PACKED BEDS WITH VARIABLE POROSITY

JHY-WEN WU and HSIN-SEN CHU†

Department of Mechanical Engineering, National Chiao Tung University, Hsinchu, Taiwan 300,
Republic of China

Abstract—The primary concern of this study deals with the prediction of thermal performance of packed beds with variable porosity. Combined conduction and radiation heat transfer in plane-parallel packed beds of spherical particles was investigated numerically. The effects of variable porosity, effective thermal conductivity, and thermal radiation were taken into account. The method for radiative transfer equation was based on the P_3-spherical harmonic approximation, while the finite-difference scheme was employed to solve the energy equation. Four different models of porosity distributions were tested. It was found that variable porosity and effective thermal conductivity effects on the mean total effective thermal conductivity and radiative heat flux distributions are important and should not be ignored. © 1999 Elsevier Science Ltd. All rights reserved.

1. INTRODUCTION

Combined conduction and radiation heat transfer in packed beds has become an increasingly important research because of its wide applications in thermal insulation systems designs. Numerous studies have been reported in relation to this topic. Tien[1] gave an overview of the existing knowledge on radiative heat transfer on packed beds. In homogenous media such as gases, absorption and emission are the major radiative mechanism. If the medium contains inhomgeneities, such as the particles on packed beds, the addition mechanism of scattering is considered. Drolen and Tien[2] predicted the radiative extinction characteristics of independent and dependent scattering in packed beds. The independent and dependent scattering regimes were shown over a wide range of size parameter, $\pi D_p/\lambda$, and solid volume fraction, fv. Singh and Kaviany[3] simulated the radiative heat transfer through a packed beds of relatively large spherical particles by the Monte Carlo method and indicated the failure and success of independent theory. Singh and Kaviany[4] showed that the dependent properties of packed beds of opaque spheres can be obtained from their independent properties by scaling the optical thickness while leaving the albedo and the phase function unchanged. The scaling factor is found to depend mainly on the porosity and is almost independent of the emissivity. Nasr et al[5] measured the temperature-dependent effective thermal conductivity of packed beds of large particles and extracted the radiative conductivity from their experimental data.

The variable porosity close to an impermeable boundary leads to a number of important effects such as boundary, inertia, and channeling. In the experimental studies of Benenati and Brosilow[6] and Ridway and Tarbuck,[7] the porosity variation near the wall region of the random beds of uniformly sized spheres shows an oscillatory behavior. The oscillation decreases going away from the wall, and approximates to a constant value. While the oscillations decrease sufficiently after the distance of approximately five particle diameters, variation of porosity with respect to volume is large such that it cannot be ignored in the region within this distance. Vafai and Tien[8] analyzed the boundary and inertia effects on convective flow and heat transfer for constant porosity media and

---

† To whom all correspondence should be addressed.

expressed them in terms of several governing parameters. These effects were further investigated by an experiment[9] for transient mass transfer through constant porosity. In some applications, such as fixed-bed catalytic reactors, packed-bed heat exchangers, drying, chemical reaction engineering and metal processing, the constant porosity assumption does not hold because of the influence of an impermeable boundary. Vafai et al[10] presented an experimental investigation on the effects of a solid impermeable boundary and variable porosity on forced convection in porous media. The heat transfer of packed beds containing a stagnant gas is a function of their solid and gas thermal conductivities, the porosity of the bed, the local temperature, and the material, shape and size of the particle. To determine heat transfer characteristics of packed beds, the radiative properties of the packed beds such as its extinction coefficient, albedo, and phase function must also be described in terms of porosity, particle size, and surface reflectivity. Lu et al[11] presented a theoretical analysis for the combined forced convection and radiation in packed beds along a flat plate. In this study, the non-Darian effects were considered for the hydrodynamics and dependent scattering effects were taken into account for the radiation transfer. The radiative and conductive properties were assumed as functions of porosity which was considered to vary exponentially with the distance from the plate. Recently, Kamiuto et al[12] while modeling the heat transfer in packed beds, classified the theoretical models into two categories: (1) the cell model, and (2) the quasi-homogeneous model. The former model could not take into account the long-range effects of radiative transfer through the voids of a packed bed, and therefore, led to serious errors on evaluating the heat transfer characteristics of a comparatively thin packed bed. Moreover, the radiative transfer through a packed bed is governed by the equation of transfer, and thus, radiative transports such as radiative heat flux may be accurately evaluated even for a comparative thin packed bed by solving the equation of transfer numerically. In their paper, the quasi-homogeneous model was developed for finding the heat transfer characteristics of packed beds at high temperatures, experimentally and theoretically, utilizing a correlated scattering theory that enables the calculation of the dependent properties of large particles from their independent properties. In addition, they also showed that results based on the uncorrelated-scattering theory always overestimate the total effective conductivities of such beds.

The objective of this study was to investigate the effects of four different porosity distributions on mean effective thermal conductivity and radiative heat flux distributions. In fact, each model has different characteristics: model 1 represents the mean porosity in the bulk region; model 2 consists of two principal equations, an order-3 polynomial expression and a damped cosine, along with the addition of a constant; model 3 is an exponential function that ignores the oscillations in porosity in the near-wall region; and model 4 uses the Bessel function as an oscillatory factor allowing consideration of the effects of damped oscillations. It was found that variable porosity distribution significantly affects the total effective thermal conductivity as well as the radiative heat flux near the walls.

2. ANALYSIS

Consider the combined conductive and radiative heat transfer in plane-parallel packed beds. Local porosity within the packed beds varies with distance from the boundary, and four different porosity distributions are symmetric with respect to the mid-plane of the packed beds. The radiative heat transfer of the packed beds are assumed as the quasi-homogenous model. The packed spheres are to be opaque with a gray diffuse surface. The radiative properties of packed beds do not depend on wavelength as is predicted by the correlated-scattering theory.[12] The two boundaries of packed beds kept at two different constant temperatures with gray diffuse emitters and reflectors are considered. The packed beds show continuous heat transfer and are in the steady state. The mathematical formulation of this problem, in the dimensionless form, is given by

$$0 = \frac{\partial}{\partial \eta}\left[\lambda_{\mathrm{m}} \frac{\partial \theta}{\partial \eta}\right] - \nabla \cdot Q^{\mathrm{r}}(\eta), \tag{1}$$

where η is the dimensionless coordinate, λ_{m} the effective thermal conductivity and Q^{r} the dimensionless radiative heat flux. The associated boundary conditions for Eq. (1) are taken as

$$\theta(0) = 1, \qquad \theta(1) = 0.5, \tag{2}$$

where θ is the dimensionless temperature. The dimensionless intensity I satisfies the radiative transfer equation which is written in the following form

$$\mu \frac{\partial I(\eta, \mu)}{\partial \eta} + \tau(\eta) I(\eta, \mu) = \tau(\eta)(1 - \omega)\theta^4(\eta) + \left[\frac{\omega\tau(\eta)}{2}\right] \int_{4\pi} I \cdot P(\mu, \mu') \, d\mu', \tag{3}$$

where I is the dimensionless radiation intensity, ω the scaled scattering albedo, P the phase function and τ the optical thickness.[9] The boundary conditions for Eq. (3) are taken as

$$I(0, \mu) = \varepsilon_h \theta^4(0) + 2(1 - \varepsilon_h) \int_0^1 I(0, -\mu') \, d\mu', \quad \mu > 0, \tag{4a}$$

$$I(1, -\mu) = \varepsilon_h \theta^4(1) + 2(1 - \varepsilon_h) \int_0^1 I(1, \mu') \, d\mu', \quad \mu > 0, \tag{4b}$$

where ε_h and ε_c are the total hemispherical emissivity of the hot and the cold wall, respectively, and μ the direction cosines in the Cartesian coordinate system.

The divergence of the dimensionless net radiative heat flux $\nabla \cdot Q^r(\eta)$ in Eq. (1) can be expressed as

$$\nabla \cdot Q^r(\eta) = \frac{\tau(\eta)(1 - \omega)}{N}\left[\theta^4(\eta) - \frac{\psi_0(\eta)}{4}\right], \tag{5}$$

where N is the conduction-to-radiation parameter, defined as $N = k_s/4\sigma T_h^3 L$.

Using the spherical-harmonic method for the solution of the radiative transfer equation for packed beds, the intensity of radiantion $I(\eta, \mu)$ and the scattering phase function $P(\mu, \mu')$ are assumed to be present in a series of Legendre polynomials.[13] Bayazitoglu and Higenyi[14] have discussed and compared the results of the P_3 approximation with exact solutions, and have shown that the P_3 approximation is quite accurate. The P_3 approximation is therefore adopted in the present investigation. For the P_3 approximation, four ordinary differential equations can be obtained as

$$\frac{\partial \psi_0}{\partial \eta} = \frac{14\tau(\eta)}{3}(1 - \omega f_3)\psi_3 - 12N\tau(\eta)(1 - \omega f_1)\psi_1, \tag{6a}$$

$$\frac{\partial \psi_1}{\partial \eta} = -\frac{\tau(\eta)}{4N}(1 - \omega f_0)\psi_0 + \frac{\tau(\eta)}{N}(1 - \omega)\theta^4, \tag{6b}$$

$$\frac{\partial \psi_2}{\partial \eta} = \frac{7\tau(\eta)}{3}(1 - \omega f_3)\psi_3, \tag{6c}$$

$$\frac{\partial \psi_3}{\partial \eta} = \frac{2\tau(\eta)}{3}(1 - \omega f_0)\psi_0 - \frac{5\tau(\eta)}{3}(1 - \omega f_2)\psi_2 - \frac{8\tau(\eta)}{3}(1 - \omega)\theta^4, \tag{6d}$$

where, by definition, $\psi_0(\eta)$ and $\psi_1(\eta)$ are the incident radiation and the radiative heat flux, respectively. $\psi_2(\eta)$ and $\psi_3(\eta)$ are the dimensionless second and third moments of the incident radiation, respectively. In the field of heat transfer, it is usually these two quantities that are of interest rather than the intensity itself. Thus, only the solution for $\psi_0(\eta)$ and $\psi_1(\eta)$ is presented here.

To be compatible with the spherical harmonic approximation, the boundary conditions of moments of the radiant intensity must be formulated using Marshak's boundary conditions. Therefore, Eqs. (4a) and (4b) become

$$\int_0^1 I(\eta, \mu)\mu^{2l-1} \, d\mu = \int_0^1 \left[\varepsilon_h \theta^4(\eta) + 2(1 - \varepsilon_h) \int_0^1 I(\eta, -\mu')\mu' \, d\mu'\right]\mu^{2l-1} \, d\mu, \quad \mu > 0, \tag{7a}$$

$$\int_0^1 I(\eta, -\mu)\mu^{2l-1} \, d\mu = \int_0^1 \left[\varepsilon_c \theta^4(\eta) + 2(1 - \varepsilon_c) \int_0^1 I(\eta, \mu')\mu' \, d\mu'\right]\mu^{2l-1} \, d\mu, \quad \mu > 0, \tag{7b}$$

where $l = 1, 2, 3, \ldots, (N + 1)/2$. Substituting Eq. (5) into Eq. (1), the energy equation becomes

$$0 = \frac{\partial}{\partial \eta}\left[\lambda_m \frac{\partial \theta}{\partial \eta}\right] - \frac{\tau(\eta)}{N}(1 - \omega)\left[\theta^4(\eta) - \frac{\psi_0(\eta)}{4}\right]. \tag{8}$$

Four ordinary differential equations, Eqs. (6a)–(6d), can be solved by using the BVPFD subroutine of a commercially available software package called IMSL. The BVPFD subroutine has been used to solve a (parameterized) system of differential equations with boundary conditions at two points, using a variable-order, variable-step-size, finite-difference method with deferred corrections. The energy equation is also solved by the finite-difference method.

2.1. Porosity distribution function

The porosity distribution within a packed bed must be determined explicitly because the optical thickness and effective thermal conductivity involve the porosity as a parameter. Four porosity distribution functions are outlined below and shown in Fig. 1:

(1) The first porosity distribution model is the bulk porosity of the packed beds, ϕ_∞.
(2) The second model is derived from the experimental data of Ridgeway and Turback[7]
    for $0 \leq \zeta \leq 0.6$,
$$\phi(\zeta) = 1 - 3.10036\zeta + 3.70243\zeta^2 - 1.24612\zeta^3,$$
    for $0.6 \leq \zeta \leq 0.5\zeta_0$,
$$\phi(\zeta) = -0.1865 \exp(-0.22\zeta_1^{1.5})\cos(7.66\zeta_1) + 0.39, \tag{9}$$

    where $\zeta = z/D_p$, $\zeta_0 = L/D_p$ and $\zeta_1 = \zeta - 0.6$. D_p is the mean diameter of packed beds, L the thickness of packed beds and z represents the distance from the wall.
(3) The third porosity distribution model is assumed to vary exponentially with the distance from the boundary surface. Damped oscillations in porosity are ignored in determining the exponential function:
$$\phi(\zeta) = \phi_\infty[1 + D\exp(-D^*\zeta)], \tag{10}$$

    where the constants D and D^* are experimental parameters taken as $D^* = -6$ and $D = (1 - \phi_\infty)/\phi_\infty$.[15]
(4) The fourth model is also derived from the experimental data of Mueller:[16]
$$\phi(\zeta) = \phi_b + (1 - \phi_b)J_0(a\zeta)e^{-b\zeta} \quad \text{for } 2.61 \leq L/D_p, \tag{11}$$

    where
$$a = 8.243 - \frac{12.98}{(L/D_p + 3.156)} \quad \text{for } 2.61 \leq L/D_p \leq 13.0,$$
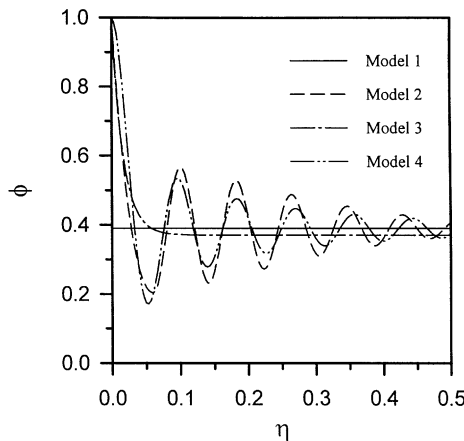$$a = 7.383 - \frac{2.932}{(L/D_p - 9.864)} \quad \text{for } 13.0 \leq L/D_p,$$

Fig. 1. Profiles of the porosity distribution function for the four models ($L/D_p = 10$).

$$b = 0.304 - \frac{0.724}{L/D_p},$$

$$\phi_b = 0.379 + \frac{0.078}{(L/D_p - 1.8)},$$

and $J_0(a\zeta)$ is a Bessel function of the first kind.

2.2. Effective thermal conductivity

Bruggeman's effective medium theory[12] is utilized in this paper. According to this theory, λ_m is given by

$$\lambda_m = (k_a/k_s)\{(\kappa - 1)\kappa^{1/3}\phi[\sqrt[3]{(\sqrt{A} - 1)/2} - \sqrt[3]{(\sqrt{A} + 1)/2}] + \kappa\}, \tag{12}$$

where $A = 1 + 4/27\phi^3(\kappa - 1)^3/\kappa^2$, and $\kappa = k_s/k_a$, here k_s and k_a are thermal conductivities of the dispersed and continuous phase of a packed bed, respectively.

2.3. Radiative properties

According to the correlated-scattering theory,[12] the scaled radiative properties for a packed bed can be described as

$$\tau = \beta L = \frac{\pi D_p^2 n_p L(2\gamma_2 - 1)}{4}$$

$$= 1.5(L/D_p)(1 - \phi)(2\gamma_2 - 1), \tag{13}$$

$$\omega = \rho_s, \tag{14}$$

where $\gamma_2 = 1 + 1.5(1 - \phi) - (3/4)(1 - \phi)^2$, β is the scaled extinction coefficient, ρ_s the hemispherical reflectivity of a packing sphere, and n_p the number density of packed spheres.

The phase function of a diffuse sphere is assumed to be represented as a series of Lengendre polynomials in the following form

$$P(\mu, \mu') = \sum_{n=0}^{3} (2f_n + 1)f_n P_n(\mu) P_n(\mu'). \tag{15}$$

2.4. Heat transfer characteristics

The dimensionless total heat flux across a packed bed is calculated from

$$Q_t = -\lambda_m(\eta)\frac{d\theta}{d\eta} + \frac{1}{2N}\int_{-1}^{1} I(\eta, \mu)\,d\mu = -K_{eff}\frac{d\theta}{d\eta}, \tag{16}$$

where K_{eff} represents the total effective thermal conductivity. This dimensionless total heat flux can be readily computed, once both the energy equation and the P_3 equations are solved. Moreover, the mean total effective thermal conductivity of a packed bed between two boundaries can be evaluated from

$$\overline{K_{eff}} = \int_{0}^{1} K_{eff}\,d\eta, \tag{17}$$

where $\overline{K_{eff}}$ represents the mean total effective thermal conductivity.

3. RESULTS AND DISCUSSION

In order to check the accuracy of the numerical method presented here, the uniform grid test for model 2 was made. The results were presented in Table 1. As is shown, the 111 uniform grid points are sufficiently accurate and can be used in all cases for the consideration of the CPU time. The predictions for different porosity models based on the P_3 approximation are compared with the experimental data by Kamiuto et al[9] in Fig. 2. The theoretical results are shown to be in good agreement with experimental results that account for the variable porosity effects. The temperature

Table 1

η \ Grid Temp.	91	111	131	151	171	191
0.0	1.0000	1.0000	1.0000	1.0000	1.0000	1.0000
0.2	0.9345	0.9343	0.9342	0.9340	0.9338	0.9335
0.4	0.8699	0.8699	0.8697	0.8695	0.8691	0.8687
0.6	0.7872	0.7874	0.7873	0.7870	0.7865	0.7860
0.8	0.6869	0.6876	0.6878	0.6877	0.6874	0.6869
1.0	0.5000	0.5000	0.5000	0.5000	0.5000	0.5000
CPU time	365.1	871.9	1655.4	2275.9	3094.9	4581.2
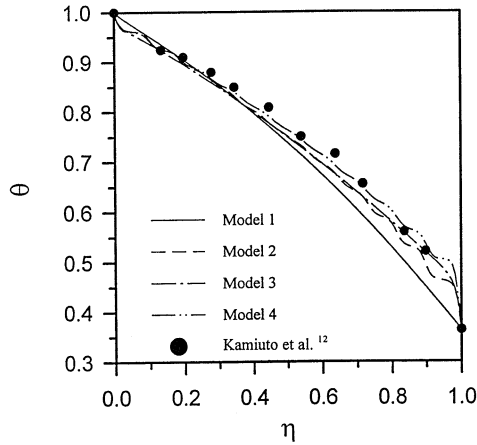
Fig. 2. Steady temperature distributions for different models when $\kappa = 781.7$, $N = 2.95$, $\omega = 0.35$, and $L/D_p = 9.82$.

profile obtained from model 4 is closer to the experimental data and obviously, that obtained from model 1 leads to a slight underprediction. Having thus gained confidence in the present numerical analysis, attempts were made to predict the effects of combined conductive and radiative heat transfer in plane-parallel packed beds of spherical particles. As shown in this figure, each model has different characteristics: model 1 represents the mean porosity in the bulk region; model 2 consists of two principal equations, an order-3 polynomial expression and a damped cosine, along with the addition of a constant; model 3 is an exponential function that ignores the oscillations in porosity in the near-wall region; and model 4 uses the Bessel function as an oscillatory factor allowing consideration of the effects of damped oscillations. A model that consists of only one principal equation would be more convenient to use in analytical packed bed transport models than one having a set of equations. As this figure shows, we cannot ignore the effects of variable porosity and conductivity in packed beds.

Figure 3 depicts the effects of κ on the effective thermal conductivity λ_m, total (radiative plus conductive) effective thermal conductivity K_{eff} and dimensionless radiative heat flux Q^r profiles with $N = 0.1$, $\omega = 0.5$, and $L/D_p = 20$ for $\kappa = 10$, $\kappa = 100$, and $\kappa = 1000$. In Fig. 3a, the profiles of λ_m of Models 2 and 4 are close to each other and so are those in models 1 and 3, but large differences occur near the hot surface because all the profiles are symmetric with respect to the mid-plane and have different characteristics. In addition, with increasing κ the effective thermal conductivity decreases sharply and becomes less sensitive to local porosity distributions, especially for the case in which $\kappa = 1000$. Here the value of κ is the ratio of the thermal conductivity of the dispersed phase to that of the continuous phase. For the influence of radiation effects, the profiles of K_{eff} shown in Fig. 3b have higher values near the hot wall than near the cold wall. The values of K_{eff} increase as κ decreases but radiation effects become stronger as κ increases. Here, the κ increase could be treated as the increase in the thermal conductivity of the dispersed phase if the thermal conductivity of continuous phase is
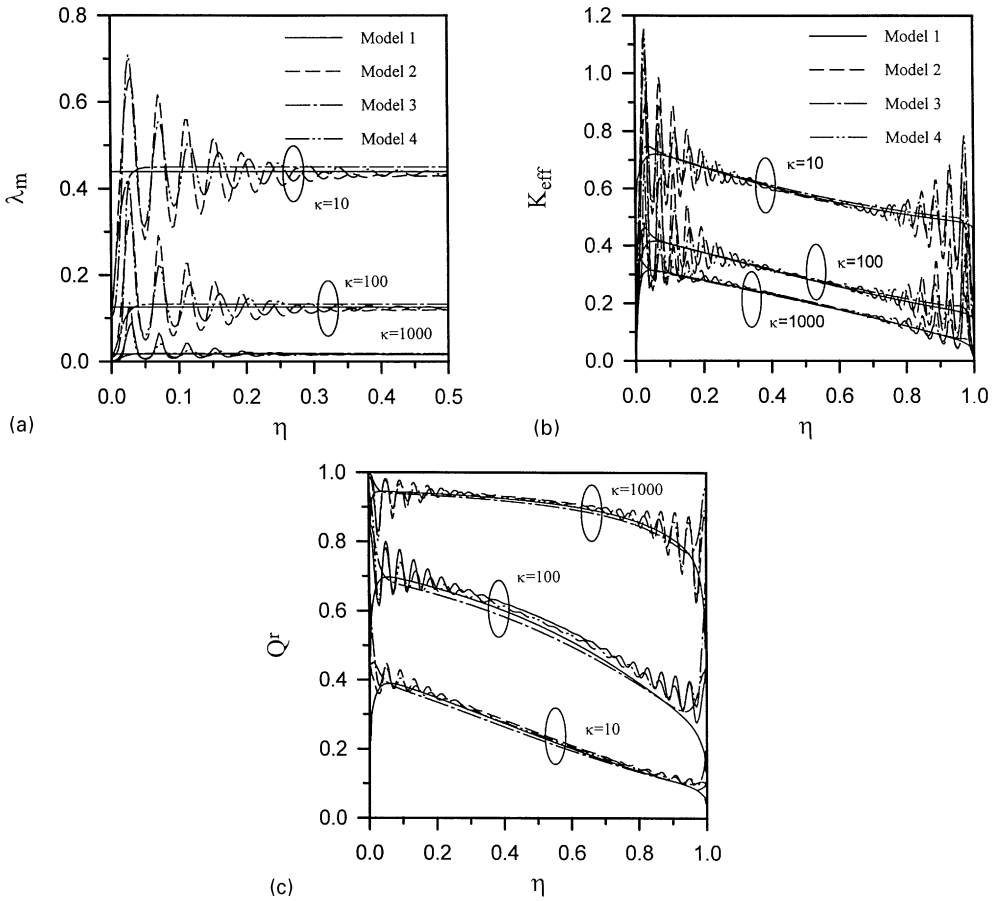
Fig. 3. (a) Effective thermal conductivity for different models when $\omega = 0.5$, $N = 0.1$, and $L/D_p = 20$. (b) Total effective thermal conductivity for different models when $\omega = 0.5$, $N = 0.1$, and $L/D_p = 20$. (c) Dimensionless radiative heat flux for different models when $\omega = 0.5$, $N = 0.1$, and $L/D_p = 20$.

fixed. When the thermal conductivity of the dispersed phase increases the temperature of the hot wall also increases at the same time because the conduction-to-radiation parameter is fixed as 0.1. This is the reason why radiative heat transfer becomes more important as increases. Figure 3c presents the dimensionless radiative heat flux. As seen in this figure, for large values of κ, radiation is the dominant mode of energy transfer and for small values of conduction dominates the heat transfer mode. The profiles for model 1 always predicts opposite results near both the surfaces because we set the porosity functions of the surface at unity except for model 1, as seen in Fig. 1. The differences between the four models are small for small values of κ because the effects of damped oscillations cause models 2 and 4 to become less sensitive.

The relationships among the mean total effective thermal conductivity $\overline{K_{eff}}$ and for all the four models are shown in Fig. 4. When κ is increased, the mean total effective thermal conductivity decreases sharply along the log scale coordinate especially from $\kappa = 1$ to $\kappa = 100$ and finally ($\kappa > 1000$) becomes a constant value of (≈ 0.197), and the differences among of the four models are small.

Figure 5 illustrate the effects of conduction-to-radiation parameter N on the total effective thermal conductivity K_{eff} and dimensionless radiative heat flux Q^r with $\kappa = 100$, $\omega = 0.5$, and $L/D_p = 20$ for, $N = 0.1$, 1, and 10. The conduction-to-radiation parameter represents the relative magnitudes of the conductive and radiative modes of heat transfer. For low values of N, radiation dominates. However, for large values of N, conduction dominates. In Fig. 5a, the K_{eff} profiles tend to approach horizontal lines for the case in which $N = 10$, when conduction dominates. Figure 5b
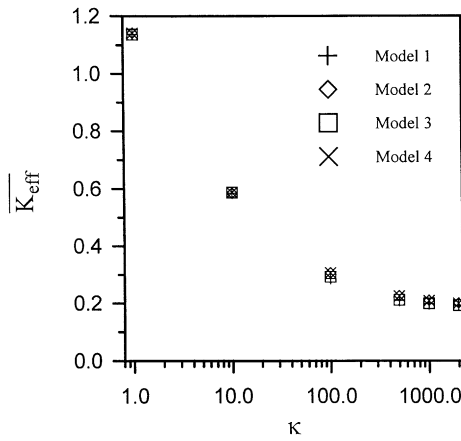
Fig. 4. Mean total effective thermal conductivity for different models when $\omega = 0.5$, $N = 0.1$, and $L/D_\mathrm{p} = 20$.
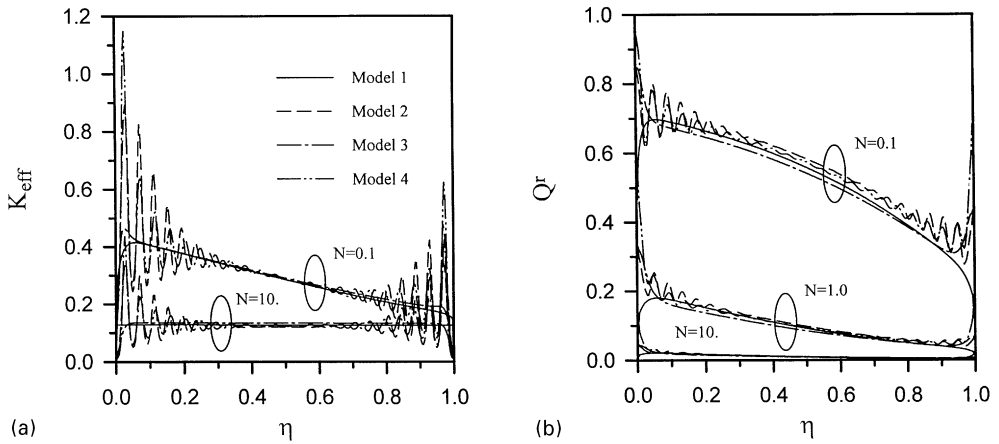

(a)   (b)

Fig. 5. (a) Effective thermal conductivity for different models when $\kappa = 100$, $\omega = 0.5$, and $L/D_\mathrm{p} = 20$.
(b) Dimensionless radiative heat flux for different models when $\kappa = 100$, $\omega = 0.5$, and $L/D_\mathrm{p} = 20$.

presents the dimensionless radiative heat flux. As expected, dimensionless radiative heat fluxes increase as N is decreased. For the case $N = 10$, radiation account for less than 5% and can be ignored. However, the differences among the four models apparently increase as N is decreased.

The relationships between the mean total effective thermal conductivity $\overline{K}_{\mathrm{eff}}$ and N are shown in Fig. 6. When N becomes larger ($N > 1$), the mean total effective thermal conductivity decreases sharply especially over the range of $N = 0.01$ to 0.1 and at last we can get a constant value of the mean total effective thermal conductivity (≈ 0.128). The differences among the four models are not evident for large N but for the case in which $N = 0.01$, the relative error is about 3.2%.

Figure 7 presents the edge effects on the profiles of K_{eff} and Q^{r} distributions when $\kappa = 100$, $\omega = 0.5$, and $N = 0.1$ for $L/D_\mathrm{p} = 10$, $L/D_\mathrm{p} = 20$, and $L/D_\mathrm{p} = 100$. In Fig. 7a, the mean total effective thermal conductivity near the hot wall increases as the ratio of thickness to particle diameter decreases. As the value of L/D_p is decreased, the effects of radiation become more pronounced. In case when $L/D_\mathrm{p} = 100$, the profiles tend to become horizontal lines, implying that the radiation effects and edge effects become less important. Figure 7b shows the radiative heat flux distributions which, as expected, have higher values because of the increase in forward scattering relative to the small value of $L/D_\mathrm{p}(= 10)$, and we can treat the small value of L/D_p as the particle diameter becomes larger for constant L and the number of damped oscillations decrease as the amplitude becomes larger in this case for models 2 and 4. From another point of view, increasing L/D_p means increasing
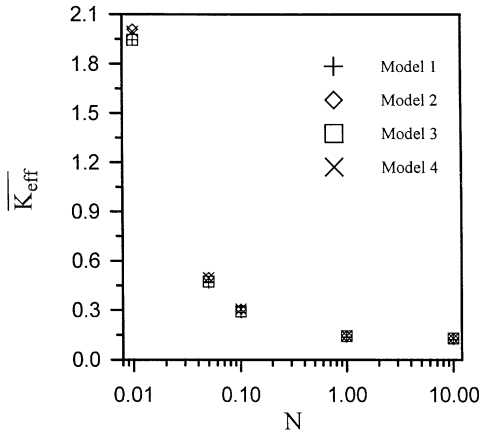
Fig. 6. Mean total effective thermal conductivity for different models when $\kappa = 100$, $\omega = 0.5$, and $L/D_p = 20$.
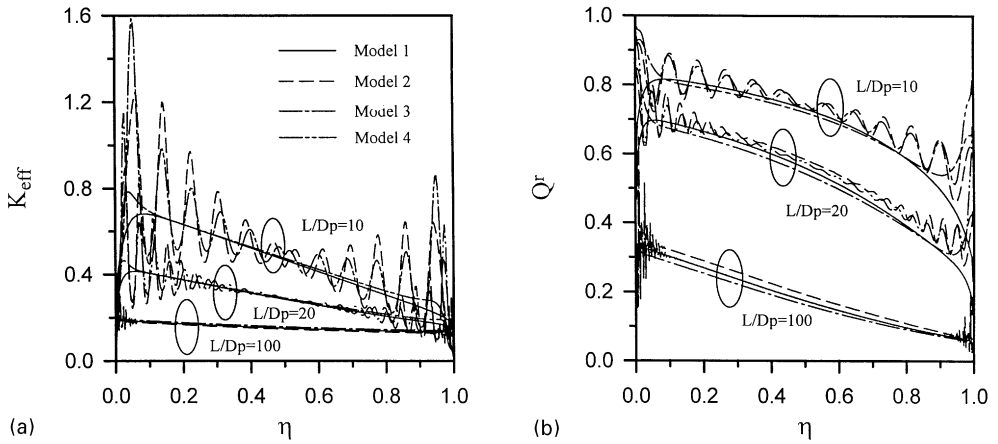
Fig. 7. (a) Total effective thermal conductivity for different models when $\kappa = 100$, $\omega = 0.5$, and $N = 0.1$. (b) Dimensionless radiative heat flux for different models when $\kappa = 100$, $\omega = 0.5$, and $N = 0.1$.
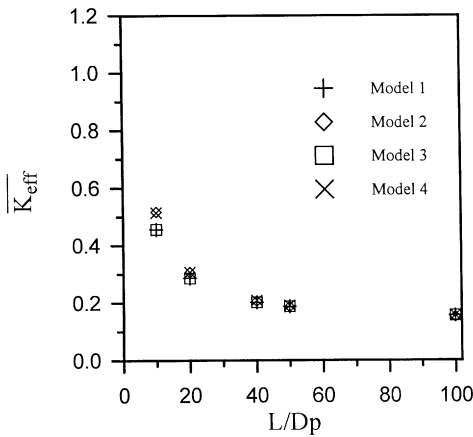
Fig. 8. Mean total effective thermal conductivity for different models when $\kappa = 100$, $\omega = 0.5$, and $N = 0.1$.

optical thickness, as defined by Eq. (13), the media tends to absorb and emit more radiation resulting in decreasing radiation effects.

The relationships between the mean total effective thermal conductivity $\overline{K_{eff}}$ and L/D_p are shown in Fig. 8. When L/D_p becomes larger ($L/D_p > 100$), the mean effective thermal conductivity decreases

and finally we get a constant value of mean total effective thermal conductivity (≈ 0.154). The differences among the four models are evident for $L/D_p = 10$. The largest differences occur at $L/D_p = 10$, the relative error is about 8.89%. Due to the different characteristics of each model, the results from model 1 are closest to mode 3 and those from model 2 are closest to model 4. We believe that according to the continuous model the range of L/D_p that was 10–100 in our work was acceptable.

4. CONCLUSION

The problem of combined conduction and radiation heat transfer in plane-parallel packed beds of spherical particles has been investigated in this work. The effects of variable porosity, effective thermal conductivity, and thermal radiation were taken into account. The P_3 approximation method was used to obtain the solutions of the equation of transfer. Four different models of porosity distribution were tested in this study. It was found that variable porosity distribution significantly affect the total effective thermal conductivity as well as the radiative heat flux near the walls. In addition, the results show that the effects of radiation become more pronounced when L/D_p decrease. When the value of L/D_p is larger than 40, the edge effects can be ignored.

REFERENCES

1. Tien, C. L., *ASME J. Heat Transfer*, 1988, **110,** 1230.
2. Drolen, B. L. and Tien, C. L., *J. Thermophys. Heat Transfer*, 1987, **1,** 63.
3. Singh, B. P. and Kaviany, M., *Int. J. Heat Mass Transfer*, 1991, **34,** 2869.
4. Singh, B. P. and Kaviany, M., *Int. J. Heat Mass Transfer*, 1992, **35,** 1397.
5. Nasr, K., Viskanta, R. and Ramadhyani, S., *ASME J. Heat Transfer*, 1994, **116,** 829.
6. Benenati, R. F. and Brosilow, C. B., *AIChE J.*, **8,** 359.
7. Ridgway, K. and Tarbuck, K. J., *J. Pharm. Pharmacol.*, 1966, **18,** 168.
8. Vafai, K. and Tien, C. L., *Int. J. Heat Mass Transfer*, 1981, **24,** 195.
9. Vafai, K. and Tien, C. L., *Int. J. Heat Mass Transfer*, 1982, **25,** 1183.
10. Vafai, K., Alkire, R. L. and Tien, C. L., *ASME J. Heat Transfer*, 1985, **107,** 642.
11. Lu, J. D., Flamant, G. and Variot, B., *Int. J. Heat Mass Transfer*, 1994, **37,** 727.
12. Kamiuto, K., Iwamoto, M. and Nagumo, Y., *J. Thermophys. Heat Transfer*, 1993, **7,** 496.
13. Özisik, M. N., *Radiative Transfer*. Wiley, New York, 1973.
14. Bayazitoglu, Y. and Higenyi, J., *J. Thermophys. Heat Transfer*, 1993, **17,** 496.
15. Hunt, M. L. and Tien, C. L., *ASME J. Heat Transfer*, 1988, **110,** 378.
16. Mueller, G. E., *Chem. Engng. Sci.*, 1991, **46,** 706.